Chemical Science

ROYAL SOCIETY OF CHEMISTRY

EDGE ARTICLE

View Article Online
View Journal | View Issue

Cite this: *Chem. Sci.*, 2024, **15**, 12589

All publication charges for this article have been paid for by the Royal Society of Chemistry

Received 18th April 2024
Accepted 27th June 2024

DOI: 10.1039/d4sc02566k

rsc.li/chemical-science

Heptacyclic aromatic hydrocarbon isomers with two azulene units fused†

Jianwen Guo,‡ Fangxin Du,‡ Bo Yu,‡ Pengcheng Du, Haoyuan Li, Jianhua Zhang and Hanshen Xin *

Azulene, known for its unique electronic properties and structural asymmetry, serves as a promising building block for the design of novel non-benzenoid polycyclic aromatic hydrocarbons (PAHs). Herein, we present the synthesis, characterization, and physical properties of three diazulene-fused heptacyclic aromatic hydrocarbons, 8,17-dioctyldiazuleno[2,1-*a*:2′,1′-*h*]anthracene (*trans* configuration), 16,18-dioctyldiazuleno[2,1-*a*:1′,2′-*j*]anthracene (*cis* configuration) and 3,18-dioctyldiazuleno[2,1-*a*:1′,2′-*i*]phenanthrene (*zigzag* configuration). Three compounds are configurational isomers with different fusing patterns of aromatic rings. All three isomers exhibit pronounced aromaticity, as revealed by nuclear magnetic resonance spectroscopy and theoretical calculations. They exhibit characteristics of both azulene and benzenoid PAHs and are much more stable than their all-benzene analogues. The optical and electrochemical properties of these three isomers were investigated through UV-vis absorption spectra and cyclic voltammetry, revealing distinct behaviors influenced by their molecular configurations. Furthermore, the isomer in *trans* configuration exhibits promising semiconducting properties with a hole mobility of up to 0.22 $cm^2 V^{-1} s^{-1}$, indicating its potential in organic electronics applications.

Introduction

Polycyclic aromatic hydrocarbons (PAHs) have been widely used as semiconducting materials due to their distinctive electronic and self-assembling properties.[1–3] Graphene, one of the most famous two-dimensional materials, which is composed of a series of alternating benzene rings, has attracted widespread attention due to its unique photoelectric and magnetic properties.[4–6] Seven-membered and five-membered rings constructed entirely of sp^2 carbons are considered defects in graphene and its nanofragments.[7,8] Numerous reports suggest that the presence of seven-membered or five-membered rings can significantly affect the physical and chemical properties, including optoelectronic properties, magnetism, chemical stability, and mechanical strength of PAHs, like those found in graphene nanofragments.[8–10] Therefore, the introduction of non-traditional conjugated structural units such as seven-membered or five-membered rings is deemed an effective method to modulate the physicochemical properties and functions of PAHs.[11–13] The design and synthesis of PAHs containing seven-membered[14–19] or five-membered[11,20–22] rings, such as azulene-fused compounds,[23–29] and the investigation of their properties and functions are becoming an emerging interdisciplinary frontier attracting widespread attention.

Azulene,[30] an aromatic bicyclic isomer of naphthalene, exhibits a substantial dipole moment of 1.08 D.[23,31] Furthermore, the non-mirror-related frontier molecular orbitals (FMOs) of azulene result in a narrow HOMO–LUMO energy gap and effectively increase the gap from the first singlet excited state (S_1) to the second singlet excited state (S_2).[32] On account of these distinctive features, azulene and its derivatives have been recognized as potential building blocks for the construction of organic electronic materials,[33–37] with a hypothesized crucial role in modulating the chemical and electronic properties of PAHs.[38–44] For example, Chi's group designed and synthesized a linear heptacyclic aromatic compound with two fused azulene units,[45] as shown in Fig. 1a. This heptacyclic aromatic compound is an isomer of heptacene (or dibenzo[*a*,*l*]pentacene), but it exhibits better air stability compared to its all benzene structural isomers.[46] However, limited methods[39] and annulation strategies exacerbate the challenges associated with synthesis and design of azulene in PAHs; thus research on azulene-fused PAHs remains relatively scarce.

In the graphene nanofragments shown in the top layer of Fig. 1b, there are three isomers with seven fused benzene rings: dinaphthaleno[2,1-*a*:2′,1′-*h*]anthracene (*trans* configuration), dinaphthaleno[2,1-*a*:1′,2′-*j*]anthracene (*cis* configuration), and dinaphthaleno[2,1-*a*:1′,2′-*i*]phenanthrene (*zigzag* configuration). Variations in condensation patterns result in distinct spatial configurations, impacting the distribution of electrons

School of Microelectronics, Shanghai University, 201800, Shanghai, China. E-mail: xinhanshen@shu.edu.cn

† Electronic supplementary information (ESI) available. CCDC 2336236. For ESI and crystallographic data in CIF or other electronic format see DOI: https://doi.org/10.1039/d4sc02566k

‡ These authors contributed equally.

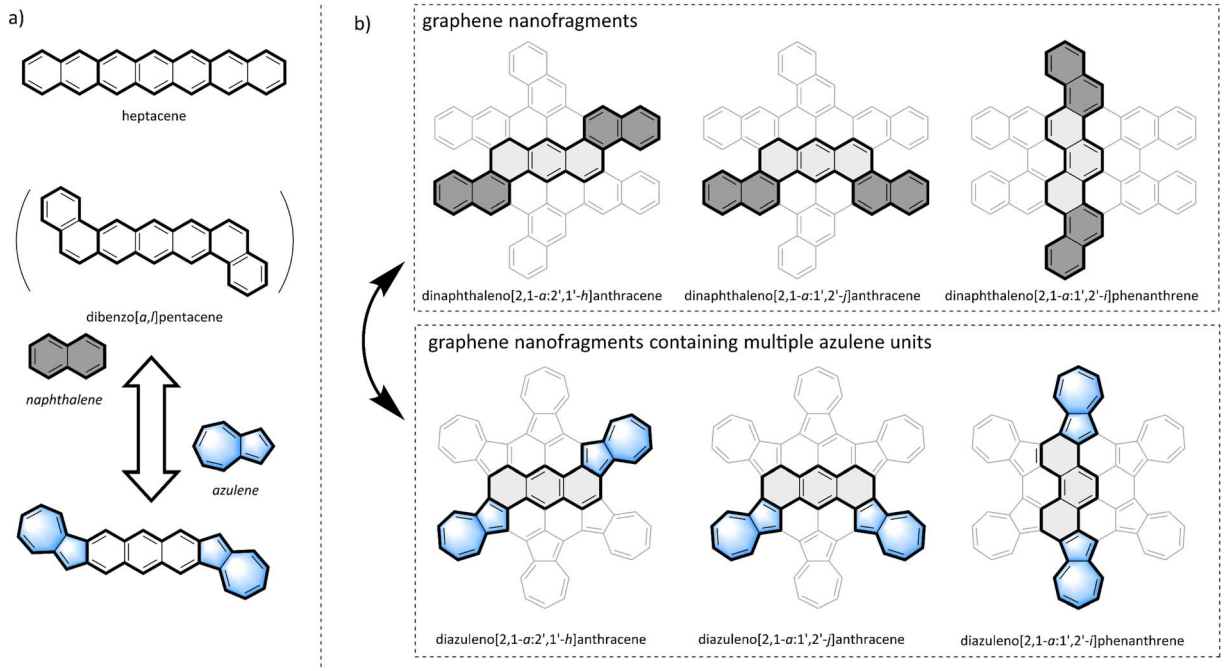

Fig. 1 (a) Chemical structures of heptacene, dibenzo[*a*,*l*]pentacene, and their azulene-fused isomers. (b) Chemical structure of graphene nanofragments containing three isomers of heptacyclic aromatic hydrocarbons (top layer) and their azulene-fused isomers (bottom).

and the structure of energy levels. These alterations are directly linked to the optical, electrical, and chemical reactivity characteristics of the molecules.[5] However, due to limitations in synthesis methods and stability issues, only dinaphthaleno[2,1-*a*:1′,2′-*i*]phenanthrene has been synthesized,[47] and studies on the other two isomers have not yet been reported. As isomers of the graphene nanofragments shown in the bottom layer of Fig. 1b, which contains multiple azulene units fused together, there also exist three isomers with seven condensed aromatic rings: diazuleno[2,1-*a*:2′,1′-*h*]anthracene (*trans* configuration), diazuleno[2,1-*a*:1′,2′-*j*]anthracene (*cis* configuration), and diazuleno[2,1-*a*:1′,2′-*i*]phenanthrene (*zigzag* configuration). Researching the synthesis, properties, and functions of this series of azulene-fused heptacyclic aromatic hydrocarbons is not only important for exploring non-benzene PAHs but also provides insights into the synthesis and application of their all-benzene PAH isomers.

In this study, we have designed and synthesized three isomers featuring the aforementioned azulene-fused heptacyclic aromatic structures (Scheme 1). Octyl groups were introduced as solubilizing chains to enhance the solubility of these PAHs, resulting in the creation of 8,17-dioctyldiazuleno[2,1-*a*:2′,1′-*h*]anthracene (**1**), 16,18-dioctyldiazuleno[2,1-*a*:1′,2′-*j*]anthracene (**2**) and 3,18-dioctyldiazuleno[2,1-*a*:1′,2′-*i*]phenanthrene (**3**). Compounds **1** and **2** are *cis–trans* configurational isomers, with two azulene units fused at both ends of an anthracene core, while compound **3** has two azulene units condensed onto a phenanthrene core, forming a *zigzag* configuration. Chemical shift changes in the ^{1}H NMR spectra among the three isomers **1–3** revealed structural properties arising from different configurations. Spectroscopic analyses, electrochemical investigations, and theoretical calculations have demonstrated that all three isomers manifest pronounced aromaticity and good redox properties. However, the differences in the fusion patterns of the aromatic rings, leading to distinct configurations, markedly affect their energy states and electron distribution profiles. Moreover, **1** shows p-type semiconducting behaviour with a high average hole mobility of 0.16 $cm^2 V^{-1} s^{-1}$ and holds great potential as a semiconductor.

Results and discussion

The synthetic routes for compounds **1–3** are depicted in Scheme 1. At the outset of the project, we strategically designed and synthesized the key intermediate **M1**. And monobromide **M2** was employed as a substrate to investigate the model reaction (Scheme 1a). Compound **S1** was synthesized *via* Friedel–Crafts acylation between 2-bromoazulene and octanoyl chloride, resulting in a yield of 57%. This was followed by a reduction using borane and boron trifluoride, providing compound **S2** [48] with a moderate yield of 59%. Subsequently, the key intermediate **M1** was prepared through a conventional Pd-catalyzed reaction between **S2** and bis(pinacolato)diboron, achieving a yield of 78%. After that, the model compound **4** was smoothly synthesized from intermediate **M1** by applying a Suzuki–Miyaura coupling reaction, followed by TMS cleavage and an annulation reaction. Since the Suzuki coupling reaction of **M1** with dibromobenzene derivatives (**M3**,[49] **M4** [50] and **M5**) was not as efficient as the reaction between **M1** and **M2**, a series of conditions were assessed to optimize the yield. As shown in Scheme 1b, by adding XPhos as a ligand, **S5** was obtained through coupling **M3** with two equivalents of **M1** in a mixed

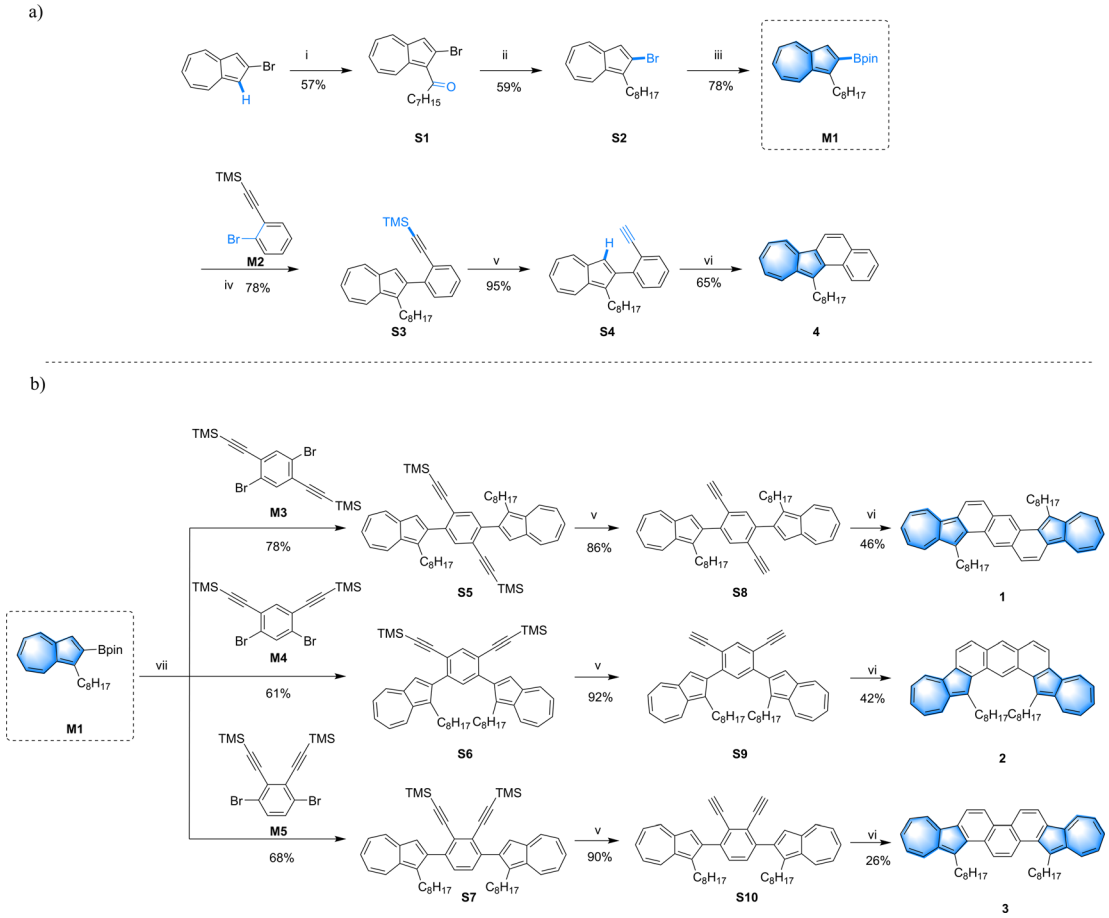

Scheme 1 Chemical structures and synthetic routes of compound **4** (a), and compounds **1–3** (b): (i) $AlCl_3$, octanoyl chloride, DCM, 0 °C; (ii) BH_3·THF, BF_3·Et_2O, THF, 0 °C to r.t.; (iii) B_2Pin_2, Pd(dppf)Cl_2, KOAc, DMSO, 80 °C; (iv) Pd$(PPh_3)_4$, K_2CO_3, toluene/EtOH/H_2O, 85 °C; (v) KF, DMF/H_2O, rt.; (vi) $PtCl_2$, toluene, 85 °C; (vii) $Pd_2(dba)_3$, XPhos, K_2CO_3, THF/H_2O, 85 °C.

solvent of THF and H_2O, affording a yield of 78%. Under the same conditions, **M1** could react with **M4** and **M5** respectively, producing **S6** and **S7** with acceptable yields. Subsequently, by treating TMS-protected precursors **S5–S7** with KF, the desilylation products **S8–S10** were obtained with yields of 86%, 92%, and 90% accordingly. Finally, the target molecules were successfully synthesized through a Pt-catalyzed double annulation reaction.[51] Compounds **1** and **2** were synthesized with medium yields of 46% and 42% respectively, while compound **3** was obtained with a lower yield of 26% *via* the same procedure. This lower yield may be attributed to the presence of two adjacent alkynyl groups in *o*-diphenylacetylene, which might hinder the coordination step in the Pt-catalyzed reaction, leading to unexpected byproducts and a reduced yield.

At room temperature, diazulene-fused isomers **1–3** with two octyl chains show good solubility in dichloromethane and aromatic solvents (>7 mg mL^{-1}), exhibiting pronounced insolubility in methanol, a characteristic that could be utilized in purification and characterization. The chemical structures of isomers **1–3** were fully characterized by nuclear magnetic resonance (NMR) spectroscopy and high-resolution mass spectrometry (HRMS). Thermogravimetric analysis (TGA) was performed under a nitrogen atmosphere to investigate the thermal properties of isomers **1–3**. As shown in Fig. S1,† TGA curves reveal the high 5 wt% decomposition temperatures of these compounds, indicating good thermodynamic stability. It can be observed that isomer **3** exhibits a higher stability (383 °C) compared to isomers **1** (308 °C) and **2** (243 °C). This may be attributed to the higher rigidity of the *zigzag* conformation of isomer **3**, while the *cis* conformation of isomer **2** exhibits lower rigidity, with higher steric hindrance between adjacent alkyl chains. As shown in Table S1 and Fig. S2,† both the single point energy calculations and independent gradient model (IGM)[52,53] results also indicate that **3** has greater thermal stability than **2** and **3** (see the ESI† for details).

As depicted in Fig. 2, the ^1H chemical shifts within the aromatic region for isomers **1–3**, as well as model compound **4**, were presented for comparison. Notably, isomer **1** features a singlet at 9.46 ppm for the ^1H_h, a characteristic attributed to its centrosymmetric structure. In contrast, isomer **2**, which possesses a C_2-symmetric structure, shows a splitting of the signal in the corresponding position into two sets ($^1H_{h'}$ and $^1H_{i'}$). Significantly, the $^1H_{i'}$ experiences a remarkable downfield shift to 10.43 ppm, an effect likely due to deshielding by the ring current in the bay region (Fig. 3d). When compared to isomers **1** and **2**, the chemical shifts for the seven-membered rings in

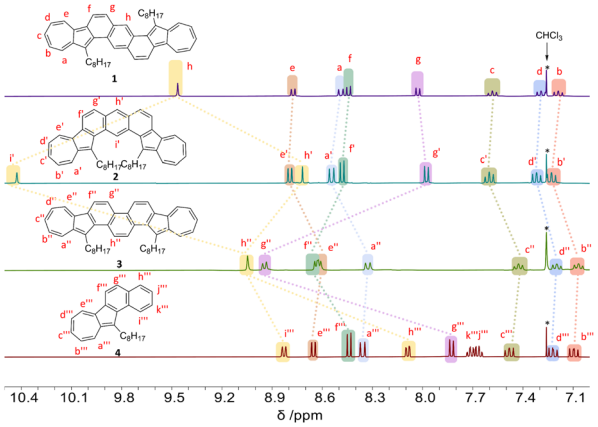

Fig. 2 ^{1}H NMR (400 MHz, $CDCl_3$, 298 K) spectra of the aromatic regions for compounds **1**, **2**, **3**, and **4**. All protons are labelled.

isomer **3** ($^{1}H_{a''}$, $^{1}H_{b''}$, $^{1}H_{c''}$, $^{1}H_{d''}$, and $^{1}H_{e''}$) shift to a higher field, indicating a decrease in aromaticity for the seven-membered rings. Specifically, in compound **3**, the chemical shifts for the $^{1}H_{f''}$ and $^{1}H_{g''}$ protons show a significant downfield shift compared to the analogous protons in compounds **1**, **2**, and **4**. This indicates that the benzene rings fused to the azulene units in compound **3** exhibit increased aromaticity compared to those in the other compounds, a conclusion that is supported by the nucleus-independent chemical shifts (NICS) calculations shown in Fig. 3c. Moreover, the central benzene ring in compound **3** has the smallest chemical shift for $^{1}H_{h'}$ among the diazulene-fused isomers and possesses the largest NICS value, indicating lower aromaticity.

The diazulene-fused structure of compound **1** was further confirmed by single crystal X-ray analysis, which was crystalized in the mixed solvents of ethylbenzene and *o*-dichlorobenzene by slowly cooling down to −20 °C. Unfortunately, compounds **2** and **3** with two ipsilateral exsolution chains are difficult to crystalize perfectly for analysis, which may be due to steric hindrance. The single crystal of compound **1** exhibits a triclinic crystal system, $P\bar{1}$ space group, with each unit cell containing only one molecule (Table S2 and Fig. S3†).

As shown in Fig. S3b,† crystallographic analysis revealed that the conjugated skeleton of compound **1** exhibits good planarity, with the maximum dihedral angle between any fused rings being 2.05°. Within each stacked column, all adjacent conjugated planes maintain a consistent π–π distance of 3.437 Å between levels (Fig. 3b). The good planarity and short packing distance may endow compound **1** with satisfactory charge mobility. As shown in Fig. S3b,† the average bond length within the skeleton of compound **1** is shorter than the expected length for a conjugated single bond between two sp^2 carbon atoms (1.45 Å) falling instead within the range of aromatic double bonds for sp^2 carbons (1.38–1.40 Å). This observation strongly supports and confirms the excellent aromaticity exhibited by compound **1**.[54] To understand the electronic structure and aromaticity of azulene-fused PAHs, NICS(1)zz (isotropic chemical shielding surface at 1 Å of the *Z* axis)[55] and anisotropy of the induced current density (ACID) calculations[56] were carried out as shown in Fig. 3. All fused rings have negative NICS(1)zz values (−9.81 to −18.31 ppm), indicating their aromatic characters. The average NICS(1)zz values of all azulene-fused PAHs are more negative than those of their all benzene-fused isomers (Fig. S4†), indicating that the incorporation of azulene units in the conjugated skeleton gently enhances its aromaticity. The strong aromaticity of these azulene-fused PAHs is also supported by the ACID plots (Fig. 3d), which display a clockwise ring current of the π electrons along the periphery. According to

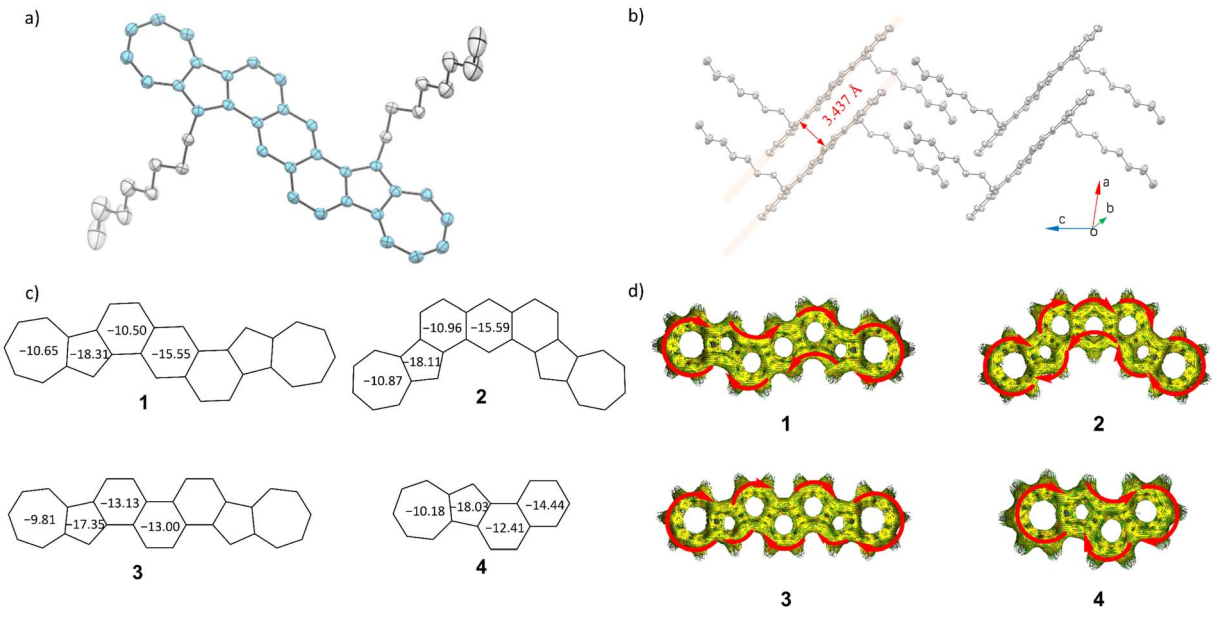

Fig. 3 (a) Thermal ellipsoids of compound **1** (probability level = 50%). (b) Packing structure of compound **1**. (c) Calculated NICS(1)zz values for compounds **1**–**4**. (d) Calculated ACID plots for compounds **1**–**4**.

the NICS(1)zz values, compared with isomer **1** and isomer **2**, isomer **3** has lower aromaticity in the azulene units and the central benzene ring, while the benzene rings adjacent to the azulene units have higher aromaticity. This result is well consistent with the NMR results. Since the aromaticity of the central rings of acenes could be overestimated using NICS values,[57,58] which may bother the study of molecular aromatics, we conducted additional analyses including multi-center index (MCI),[59] fluctuation index (FLU),[60] harmonic oscillator model of aromaticity (HOMA),[61] and normalized multicenter bond order (NCBO)[62] to provide a more comprehensive assessment of the aromatic nature of compounds **1–4**. As shown in Table S3,† the results from MCI, FLU, HOMA, and NCBO all indicate that the aromaticity of the central ring in compounds **1–3** is consistent with the NICS(1)zz values.

The optical and electrochemical properties of three diazulene-fused heptacyclic dyes **1–3** and the tetracene analogue **4** were investigated using UV-vis absorption spectra and cyclic voltammetry (CV) measurements. The corresponding data are summarized in Table 1. As shown in Fig. 4a, the absorption spectra obtained in dichloromethane show that compounds **1–3** exhibit strong absorbance from 300 to 600 nm, accompanied by weaker absorption bands from 600 to 900 nm, as anticipated. The strong absorbance arises from the π–π* transition of the conjugated system, while the weaker absorption bands from 600 to 900 nm represent a characteristic "azulene type" structured absorption profile, originating from the S_0 to S_1 transitions of azulene moieties. Compared to compound **4** with lower degrees of conjugation, the absorption of compounds **1**, **2**, and **3** was enhanced and a remarkable bathochromic shift has been observed. Notably, within the strong absorbance range, isomer **2** exhibits two distinct absorption bands (300–400 nm with a peak at 352 nm; $\varepsilon = 5.29 \times 10^4\ M^{-1}\ cm^{-1}$, and 400–550 nm with peaks at 417, 439, and 466 nm), in contrast to **1** (peak at 402 nm; $\varepsilon = 4.49 \times 10^4\ M^{-1}\ cm^{-1}$) and **3** (peak at 378 nm; $\varepsilon = 5.51 \times 10^4\ M^{-1}\ cm^{-1}$). This difference may stem from the unique *cis* configuration of isomer **2**, which facilitates specific electronic transition pathways. This observation aligns with time-dependent density functional theory (TD-DFT) calculations (Fig. S5†). Furthermore, compared to isomers **1** and **2**, isomer **3** exhibits fewer absorption peaks in the 300–500 nm range, with only a shoulder peak at 427 nm. This may be due to the *zigzag* configuration having greater structural rigidity compared to the *trans* and *cis* configurations, which reduces the coupling between electronic

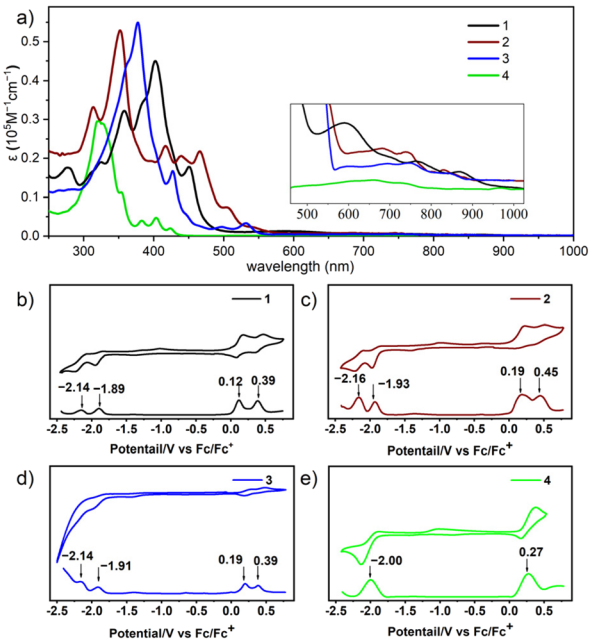

Fig. 4 (a) UV-vis absorption (10^{-6} M in DCM). Cyclic voltammetry (CV) curves and differential pulse voltammetry (DPV) curves of (b) **1**, (c) **2**, (d) **3**, and (e) **4**, measured in 0.1 M solution of $^nBu_4NPF_6$ in DCM.

transitions and molecular vibrational states. Besides, in the *zigzag* configuration, π electrons may be more evenly distributed across the molecular framework. This result is consistent with NICS(1)zz calculations, which show a more uniform distribution of values across the rings in isomer **3** (Fig. 3c). As shown in Fig. S6,† the absorption of compounds **1**, **2**, and **4** in the film is like their absorption in dichloromethane, with their maximum absorption wavelength red-shifted by about 6 nm; whereas the absorption of compound **3** in the film, compared to its solution absorption, has significantly blue-shifted by about 50 nm. These observations indicate that compound **3** tends to form H-aggregates in a solid state, while the other molecules tend to form J-aggregates.[63] Although azulene exhibits atypical fluorescence that follows the anti-Kasha rule,[22] we studied the emission properties of compounds **1–4** and observed no detectable fluorescence. As shown in Fig. S7,† compounds **1**, **2**, and **3** exhibit good photostability (half-life time $t_{1/2}$: 25 days, 34 days, and 26 days, respectively) under ambient air and light conditions as compared to their all benzene-fused counterparts

Table 1 Optical, electrochemical and DFT calculation data

Cp. ID	λ_{max}^{abs} [a]	λ_{onset} [a]	E^{ox} [b]		E^{red} [b]		E_{HOMO}^{cv} [c]	E_{LUMO}^{cv} [c]	E_g^{cv} [c]	E_g^{opt} [c]	E_{HOMO}^{cal} [d]	E_{LUMO}^{cal} [d]	E_g^{cal} [d]
1	402 and 751	935	0.12	0.39	−2.14	−1.89	−4.92	−2.91	2.01	1.32	−4.52	−2.23	2.29
2	352, 417, and 682	912	0.19	0.45	−2.16	−1.93	−4.99	−2.87	2.13	1.36	−4.64	−2.08	2.56
3	378 and 748	918	0.19	0.39	−2.14	−1.91	−4.98	−2.89	2.11	1.35	−4.59	−2.20	2.39
4	321 and 660	435	0.27		−2.00		−5.07	−2.80	2.27	2.85	−4.77	−2.03	2.74

[a] Measured in 1×10^{-5} M DCM solutions. [b] Measured in $^nBu_4NPF_6$ solution *vs.* Ag/AgCl (calibration using ferrocene), $E^{ox/red}$ acquired from DPV curves. [c] Calculated from $E_{HOMO/LUMO} = -(E^{ox/red} + 4.8)$, $E_g^{cv} = E_{LUMO}^{cv} - E_{HOMO}^{cv}$, $E_g^{opt} = 1240/\lambda_{onset}$. [d] Estimated from DFT calculations.

and other azulene-fused PAHs.[45] The electrochemical properties of three diazulene-fused heptacyclic aromatics **1–3** and the model compounds **4** were studied with cyclic voltammetry (CV) and differential pulse voltammetry (DPV) in DCM. As shown in Fig. 4, isomers **1–3**, with two azulenes fused, unambiguously exhibit two oxidation waves and two reduction waves, whereas compound **4**, with one azulene fused, only shows one oxidation wave and one reduction wave. Based on the peaks of the DPV, the HOMO/LUMO energy levels of compounds **1–3** were calculated respectively and are listed in Table 1. The HOMO/LUMO energies for isomers **1**, **2**, and **3** were estimated to be −4.92/−2.91, −4.99/−2.87, and −4.98/−2.89 eV, respectively. Consequently, the electrochemical gap for isomers **1**, **2**, and **3** was calculated to be 2.01, 2.13, and 2.11 eV, respectively. The results indicate that, although all three isomers consist of two azulene units and three benzene rings as 30π electron systems, different configurations have a significant impact on their redox properties.

DFT calculations were carried out to investigate the structural and electronic properties of azulene-fused PAHs using the RB3LYP/6-31G(d,p) level of theory. The calculated data are shown in the ESI,† and the conclusions are listed in Table 1. The energy gaps estimated from calculations are larger than those obtained from DPV measurements and UV-vis spectra. Although the results are slightly varied, the data are consistent with the experiment results in trend. Consistent with the single crystal diffraction analysis results of compound **1**, all azulene-fused PAHs exhibit planar geometry with two octyl chains distributed on both sides of the scaffold plane. The electron density distribution of both HOMOs and LUMOs is delocalized over the whole backbone. As shown in Fig. 5, azulene moieties possess more contribution to LUMOs, while central backbones contribute significantly to HOMOs. It is worth noting that the HOMO electron density distribution of isomer **3** is more uniformly delocalized across the entire skeleton compared to isomers **1** and **2**, which results in a more singular path and energy change for electron transitions. Therefore, the UV-vis absorption spectrum of isomer **3** exhibits fewer fine peaks (Fig. 4a). And the NICS(1)zz value of six-membered rings in isomer **3** is more equal.

Azulene is an acid-sensitive compound, which can be protonated by strong acids such as trifluoroacetic acid (TFA) and trifluoromethanesulfonic acid (TfOH).[24,64–70] This protonation disrupts the conjugated system by attaching a proton, resulting in the formation of a stable azulenium cation. The original structure can be restored by adding a base. To clarify the protonation behaviour of diazulene-fused PAHs **1–3**, UV-vis absorption spectroscopy and ^{1}H NMR analyses were conducted. As illustrated in Fig. S8,† with an increase in TFA equivalents, the intensity of characteristic peaks of the three isomers in the 300–500 nm range gradually decreases, while a new absorption peak that gradually strengthens appears in the long-wavelength area. Notably, the absorption spectra of protonated **1–3** also show significant differences. The new absorption peak for $\mathbf{1}^{2+}$ appears in the 500–800 nm range, for $\mathbf{2}^{2+}$ in the 600–900 nm range, and for $\mathbf{3}^{2+}$ in the 450–600 nm range; therefore, the colours of $\mathbf{1}^{2+}$, $\mathbf{2}^{2+}$, and $\mathbf{3}^{2+}$ in dichloromethane solution are purple, amaranth, and orange respectively. These results indicate that upon acid addition, all three isomers form azulenium cations (Fig. 6c), and the azulenium cations remain conjugated with the fused benzene rings. However, due to different connection positions ($\mathbf{1}^{2+}$ *vs.* $\mathbf{2}^{2+}$) and different fused configurations (anthracene *vs.* phenanthrene), the π electron structures of $\mathbf{1}^{2+}$, $\mathbf{2}^{2+}$, and $\mathbf{3}^{2+}$ are distinctly different. This result can also be further confirmed using fluorescence spectra, as shown in Fig. 6b, where the emission peak of $\mathbf{1}^{2+}$ is at 650 nm, that of $\mathbf{2}^{2+}$ is at 640 nm, and that of $\mathbf{3}^{2+}$ shifts to 580 nm. As shown in Fig. S9,† the changed chemical shift can be restored by adding TEA, indicating that the protonated molecules have good stability.

Based on its conjugated π structure, short π–π stacking distance (3.437 Å), and the suitable configuration with two alkyl chains distributed on both sides, isomer **1** was selected for investigation of its charge transport properties in organic field effect transistors (OFETs). Thin film transistors of **1** were fabricated by drop-casting toluene solutions (0.5 mg mL^{-1}) onto octadecyl trichlorosilane (OTS)-treated Si/SiO_2 substrates. Au source/drain electrodes were deposited on the thin film by vacuum evaporation, resulting in a bottom gate contact (BGBC) device structure. As shown in Fig. 7, devices based on isomer **1**

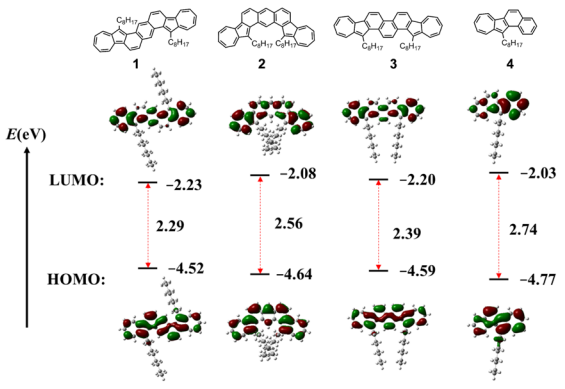

Fig. 5 Frontier molecular orbitals and their energies of compounds **1–4**, obtained using DFT calculations.

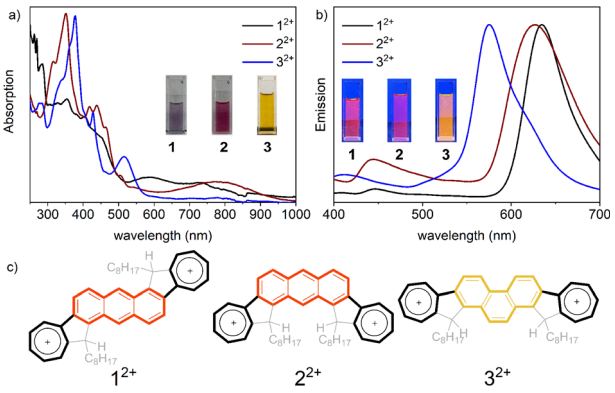

Fig. 6 Protonation behaviour: (a) UV-vis absorption and (b) emission of protonated compounds **12+**, $\mathbf{2}^{2+}$, and $\mathbf{3}^{2+}$. Insets show photos of the solutions. (c) The structure of protonated compounds.

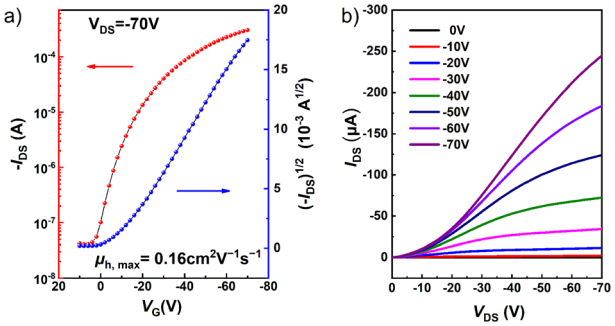

Fig. 7 (a) Transfer and (b) output curves of the OEFT device of **1**.

function as typical p-type semiconductors, which correlates well with the energy of its frontier orbitals. The average hole mobility (μ_h) extracted from the transfer curves is 0.16 cm^2 V^{-1} s^{-1} with a current on/off ratio (I_{on}/I_{off}) of 10^4–10^5 and a low threshold voltage (V_{th}) of less than 5 V. Furthermore, the highest μ_h is 0.22 cm^2 V^{-1} s^{-1}, ranking among the highest hole mobilities for PAH-based thin film OFETs.[20,22,71–76] These results demonstrate that compound **1** is a promising material for organic semiconductors.

Conclusions

In summary, three diazulene-fused heptacyclic aromatic hydrocarbons were designed, synthesized, and characterized. The structures of the three isomers **1–3** were unambiguously confirmed by nuclear magnetic resonance (NMR) spectroscopy and high-resolution mass spectrometry (HRMS). Compound **1** was further confirmed by single crystal X-ray diffraction analysis. The isomers **1–3** all exhibited excellent thermal and ambient stability, as well as good redox properties. Nuclear independent chemical shift (NICS) and anisotropy of induced current density (ACID) calculations have shown that all three isomers exhibit strong aromaticity. UV-visible absorption, electrochemical voltammetry, and theoretical calculations demonstrated that the different configurations of these isomers result in distinct optical and electrochemical properties. Additionally, isomer **1** demonstrates promising performance in OFETs with a hole mobility of up to 0.22 cm^2 V^{-1} s^{-1}, making it among the best PAHs for thin film OFETs. This showcases the potential of diazulene-fused PAHs in future electronic devices. Our studies not only expand the library of PAHs but also provide valuable insights into designing materials with distinct properties for specific applications.

Data availability

The data supporting this article have been included as part of the ESI.†

Author contributions

H. Xin designed the study and supervised the project. J. Guo, F. Du, and B. Yu conducted the experiments. P. Du, H. Li, and J. Zhang collected and analysed the data. All authors discussed the results and co-wrote the manuscript.

Conflicts of interest

There are no conflicts to declare.

Acknowledgements

This research was financially supported by the National Natural Science Foundation of China (No. 22101170) and Shanghai University. We thank Prof. Xike Gao and Dr Junjun Xiang at SIOC for helpful discussions. We thank Wenwen Zhang and Jinheng Pan (Mass Spectrometry & Metabolomics Core Facility of Westlake University) for MS analysis.

Notes and references

1 J. E. Anthony, *Chem. Rev.*, 2006, **106**, 5028–5048.
2 A. Artigas, D. Hagebaum-Reignier, Y. Carissan and Y. Coquerel, *Chem. Sci.*, 2021, **12**, 13092–13100.
3 T. Dumslaff, Y. Gu, G. M. Paternò, Z. Qiu, A. Maghsoumi, M. Tommasini, X. Feng, F. Scotognella, A. Narita and K. Müllen, *Chem. Sci.*, 2020, **11**, 12816–12821.
4 J. Wu, W. Pisula and K. Müllen, *Chem. Rev.*, 2007, **107**, 718–747.
5 X.-Y. Wang, X. Yao and K. Müllen, *Sci. China: Chem.*, 2019, **62**, 1099–1144.
6 L. Ruan, W. Luo, H. Zhang, P. Liu, Y. Shi and P. An, *Chem. Sci.*, 2024, **15**, 1511–1519.
7 H. J. Park, J. Meyer, S. Roth and V. Skákalová, *Carbon*, 2010, **48**, 1088–1094.
8 T. Björkman, S. Kurasch, O. Lehtinen, J. Kotakoski, O. V. Yazyev, A. Srivastava, V. Skakalova, J. H. Smet, U. Kaiser and A. V. Krasheninnikov, *Sci. Rep.*, 2013, **3**, 3482.
9 B. P. Klein, S. E. Harman, L. Ruppenthal, G. M. Ruehl, S. J. Hall, S. J. Carey, J. Herritsc, M. Schmid, R. J. Maurer, R. Tonner, C. T. Campbell and J. M. Gottfried, *Chem. Mater.*, 2020, **32**, 1041–1053.
10 C. M. Cruz, S. Castro-Fernández, E. Maçôas, A. Millán and A. G. Campaña, *Synlett*, 2019, **30**, 997–1002.
11 K. Kawasumi, Q. Zhang, Y. Segawa, L. T. Scott and K. Itami, *Nat. Chem.*, 2013, **5**, 739–744.
12 Y. Fei and J. Liu, *Adv. Sci.*, 2022, **9**, 2201000.
13 Q. Fan, D. Martin-Jimenez, D. Ebeling, C. K. Krug, L. Brechmann, C. Kohlmeyer, G. Hilt, W. Hieringer, A. Schirmeisen and J. M. Gottfried, *J. Am. Chem. Soc.*, 2019, **141**, 17713–17720.
14 T. Maekawa, H. Ueno, Y. Segawa, M. M. Haley and K. Itami, *Chem. Sci.*, 2016, **7**, 650–654.
15 J. Wang, F. G. Gámez, J. Marín-Beloqui, A. Diaz-Andres, X. Miao, D. Casanova, J. Casado and J. Liu, *Angew. Chem., Int. Ed.*, 2023, **62**, e202217124.
16 R. Liu, Y. Fu, F. Wu, F. Liu, J. J. Zhang, L. Yang, A. A. Popov, J. Ma and X. Feng, *Angew. Chem., Int. Ed.*, 2023, **62**, e202219091.

17 S. Zank, J. M. Fernandez-Garcia, A. J. Stasyuk, A. A. Voityuk, M. Krug, M. Sola, D. M. Guldi and N. Martin, *Angew. Chem., Int. Ed.*, 2022, **61**, e202112834.
18 J. P. Mora-Fuentes, M. D. Codesal, M. Reale, C. M. Cruz, V. G. Jiménez, A. Sciortino, M. Cannas, F. Messina, V. Blanco and A. G. Campaña, *Angew. Chem., Int. Ed.*, 2023, **62**, e202301356.
19 I. R. Márquez, S. Castro-Fernández, A. Millán and A. G. Campaña, *Chem. Commun.*, 2018, **54**, 6705–6718.
20 L. Qin, Y. Y. Huang, B. Wu, J. Pan, J. Yang, J. Zhang, G. Han, S. Yang, L. Chen, Z. Yin, Y. Shu, L. Jiang, Y. Yi, Q. Peng, X. Zhou, C. Li, G. Zhang, X. S. Zhang, K. Wu and D. Zhang, *Angew. Chem., Int. Ed.*, 2023, **62**, e202304632.
21 Q. Jiang, T. Tao, H. Phan, Y. Han, T. Y. Gopalakrishna, T. S. Herng, G. Li, L. Yuan, J. Ding and C. Chi, *Angew. Chem., Int. Ed.*, 2018, **57**, 16737–16741.
22 X. Yang, X. Shi, N. Aratani, T. P. Gonçalves, K.-W. Huang, H. Yamada, C. Chi and Q. Miao, *Chem. Sci.*, 2016, **7**, 6176–6181.
23 H. Xin and X. Gao, *ChemPlusChem*, 2017, **82**, 945–956.
24 E. Amir, M. Murai, R. J. Amir, J. S. C. Jr., M. L. Chabinyc and C. J. Hawker, *Chem. Sci.*, 2014, **5**, 4483–4489.
25 K. Horii, R. Kishi, M. Nakano, D. Shiomi, K. Sato, T. Takui, A. Konishi and M. Yasuda, *J. Am. Chem. Soc.*, 2022, **144**, 3370–3375.
26 J. Ma, Y. Fu, E. Dmitrieva, F. Liu, H. Komber, F. Hennersdorf, A. A. Popov, J. J. Weigand, J. Liu and X. Feng, *Angew. Chem., Int. Ed.*, 2020, **59**, 5637–5642.
27 K. Biswas, Q. Chen, S. Obermann, J. Ma, D. Soler-Polo, J. Melidonie, A. Barragán, A. Sánchez-Grande, K. Lauwaet, J. M. Gallego, R. Miranda, D. Écija, P. Jelínek, X. Feng and J. I. Urgel, *Angew. Chem., Int. Ed.*, 2024, **63**, e202318185.
28 N. Ogawa, Y. Yamaoka, H. Takikawa, K. I. Yamada and K. Takasu, *J. Am. Chem. Soc.*, 2020, **142**, 13322–13327.
29 Y. Liang, S. Wang, M. Tang, L. Wu, L. Bian, J. Liang, Z. B. Tang, J. Liu, A. Guan and Z. Liu, *Angew. Chem., Int. Ed.*, 2023, **62**, e202218839.
30 A. G. Anderson and B. M. Steckler, *J. Am. Chem. Soc.*, 1959, **81**, 4941–4946.
31 D. M. Lemal and G. D. Goldman, *J. Chem. Educ.*, 1988, **65**, 923–925.
32 D. Dunlop, L. Ludvíková, A. Banerjee, H. Ottosson and T. Slanina, *J. Am. Chem. Soc.*, 2023, **145**, 21569–21575.
33 B. Hou, Z. Zhou, C. Yu, X.-S. Xue, J. Zhang, X. Yang, J. Li, C. Ge, J. Wang and X. Gao, *ACS Macro Lett.*, 2022, **11**, 680–686.
34 F. Schwarz, M. Koch, G. Kastlunger, H. Berke, R. Stadler, K. Venkatesan and E. Lörtscher, *Angew. Chem., Int. Ed.*, 2016, **55**, 11781–11786.
35 A. Diaz-Andres, J. Marín-Beloqui, J. Wang, J. Liu, J. Casado and D. Casanova, *Chem. Sci.*, 2023, **14**, 6420–6429.
36 M. H. Garner, J. T. Blaskovits and C. Corminboeuf, *Chem. Sci.*, 2023, **14**, 10458–10466.
37 J. Spengler, C. Zhu, K. Shoyama and F. Würthner, *Chem. Sci.*, 2023, **14**, 10861–10866.
38 T. Shoji, T. Okujima and S. Ito, *Int. J. Mol. Sci.*, 2020, **21**, 7087.
39 H. Xin, B. Hou and X. Gao, *Acc. Chem. Res.*, 2021, **54**, 1737–1753.
40 C. Duan, J. Zhang, J. Xiang, X. Yang and X. Gao, *Angew. Chem., Int. Ed.*, 2022, **61**, e202201494.
41 S. Wang, M. Tang, L. Wu, L. Bian, L. Jiang, J. Liu, Z. B. Tang, Y. Liang and Z. Liu, *Angew. Chem., Int. Ed.*, 2022, **61**, e202205658.
42 H. Xin, J. Li, X. Yang and X. Gao, *J. Org. Chem.*, 2019, **85**, 70–78.
43 H. Xin, J. Li, R.-Q. Lu, X. Gao and T. M. Swager, *J. Am. Chem. Soc.*, 2020, **142**, 13598–13605.
44 C. Duan, J. Zhang, S. Cai, J. Xiang, X. Yang and X. Gao, *Eur. J. Org Chem.*, 2023, **26**, e202201347.
45 A. Ong, T. Tao, Q. Jiang, Y. Han, Y. Ou, K. W. Huang and C. Chi, *Angew. Chem., Int. Ed.*, 2022, **61**, e202209286.
46 M. M. Payne, S. R. Parkin and J. E. Anthony, *J. Am. Chem. Soc.*, 2005, **127**, 8028–8029.
47 F. B. Mallory, K. E. Butler, A. C. Evans, E. J. Brondyke, C. W. Mallory, C. Yang and A. Ellenstein, *J. Am. Chem. Soc.*, 1997, **119**, 2119–2124.
48 B. Yu, P. Du, J. Guo, H. Xin and J. Zhang, *Chin. Chem. Lett.*, 2024, **35**, 109321.
49 K. Takimiya, Y. Konda, H. Ebata, N. Niihara and T. Otsubo, *J. Org. Chem.*, 2005, **70**, 10569–10571.
50 D. T. Y. Bong, E. W. L. Chan, R. Diercks, P. I. Dosa, M. M. Haley, A. J. Matzger, O. S. Miljanic and K. P. C. Vollhardt, *Org. Lett.*, 2004, **6**, 2249–2252.
51 M. B. Goldfinger and T. M. Swager, *J. Am. Chem. Soc.*, 1994, **116**, 7895–7896.
52 T. Lu and Q. Chen, *J. Comput. Chem.*, 2022, **43**, 539–555.
53 C. Lefebvre, G. Rubez, H. Khartabil, J. C. Boisson, J. Contreras-Garcia and E. Henon, *Phys. Chem. Chem. Phys.*, 2017, **19**, 17928–17936.
54 R. B. Campbell, J. M. Robertson and J. Trotter, *Acta Crystallogr.*, 1962, **15**, 289–290.
55 P. v. R. Schleyer, C. Maerker, A. Dransfeld, H. Jiao and N. J. R. v. E. Hommes, *J. Am. Chem. Soc.*, 1996, **118**, 6317–6318.
56 D. Geuenich, K. Hess, F. Köhler and R. Herges, *Chem. Rev.*, 2005, **105**, 3758–3772.
57 G. Portella, J. Poater, J. M. Bofill, P. Alemany and M. Solà, *J. Org. Chem.*, 2005, **70**, 2509–2521.
58 T. M. Krygowski, M. K. Cyrañski, Z. Czarnocki, G. Häfelingerb and A. R. Katritzky, *Tetrahedron Lett.*, 2000, **56**, 1783–1796.
59 M. Giambiagi, M. S. d. Giarnbiagi and K. C. Mundirn, *Struct. Chem.*, 1990, **1**, 423–427.
60 E. Matito, M. Duran and M. Solà, *J. Chem. Phys.*, 2005, **122**, 14109.
61 J. Kruszewski and T. M. Krygowski, *Tetrahedron Lett.*, 1972, **13**, 3839–3842.
62 E. Matito, *Phys. Chem. Chem. Phys.*, 2016, **18**, 11839–11846.
63 F. Würthner, T. E. Kaiser and C. R. Saha-Möller, *Angew. Chem., Int. Ed.*, 2011, **50**, 3376–3410.
64 K. H. Grellmann, E. Heilbronner, P. Seiler and A. Wellerla, *J. Am. Chem. Soc.*, 1968, **16**, 4238–4242.

65 N. Kihara, H. Nakayama and T. Fukutomi, *Macromolecules*, 1997, **30**, 6385–6387.
66 E. Amir, R. J. Amir, L. M. Campos and C. J. Hawker, *J. Am. Chem. Soc.*, 2011, **133**, 10046–10049.
67 M. Murai, E. Amir, R. J. Amira and C. J. Hawker, *Chem. Sci.*, 2012, **3**, 2721–2725.
68 K. Tsurui, M. Murai, S. Y. Ku, C. J. Hawker and M. J. Robb, *Adv. Funct. Mater.*, 2014, **24**, 7338–7347.
69 M. Murai, S.-Y. Ku, N. D. Treat, M. J. Robb, M. L. Chabinyca and C. J. Hawker, *Chem. Sci.*, 2014, **5**, 3753–3760.
70 A. G. Lvov and A. Bredihhin, *Org. Biomol. Chem.*, 2021, **19**, 4460–4468.
71 K. Yamamoto, Y. le, N. Tohnai, F. Kakiuchi and Y. Aso, *Sci. Rep.*, 2018, **8**, 17663.
72 H. Lee, Y. Zhang, L. Zhang, T. Mirabito, E. K. Burnett, S. Trahan, A. R. Mohebbi, S. C. B. Mannsfeld, F. Wudlb and A. L. Briseno, *J. Mater. Chem. C*, 2014, **2**, 3361–3366.
73 K. Y. Cheung, X. Xu and Q. Miao, *J. Am. Chem. Soc.*, 2015, **137**, 3910–3914.
74 S. H. Pun, Y. Wang, M. Chu, C. K. Chan, Y. Li, Z. Liu and Q. Miao, *J. Am. Chem. Soc.*, 2019, **141**, 9680–9686.
75 D. Geng, K. Wang, L. Li, K. Myny, A. Nathan, J. Jang, Y. Kuo and M. Liu, *Nat. Electron.*, 2023, **6**, 963–972.
76 K. Sekine, J. Schulmeister, F. Paulus, M. Rudolph, J. Zaumseil, K. P. Goetz, F. Rominger and A. S. K. Hashmi, *Chem.–Eur. J.*, 2019, **25**, 216–220.